Accepted April 2, 2013, for publication in the Astrophysical Journal Letters
Preprint typeset using LaTeX style emulateapj v. 5/2/11

MOLYBDENUM, RUTHENIUM, AND THE HEAVY R-PROCESS ELEMENTS IN MODERATELY METAL-POOR MAIN-SEQUENCE TURNOFF STARS

Ruth C. Peterson[1]
[1]Astrophysical Advances
Accepted April 2, 2013, for publication in the Astrophysical Journal Letters

ABSTRACT

The ratios of elemental abundances observed in metal-poor stars of the Galactic halo provide a unique present-day record of the nucleosynthesis products of its earliest stars. While the heaviest elements were synthesized by the r- and s-processes, dominant production mechanisms of light trans-ironic elements were obscure until recently. This work investigates further our 2011 conclusion that the low-entropy regime of a high-entropy wind (HEW) produced molybdenum and ruthenium in two moderately metal-poor turnoff stars that showed extreme overabundances of those elements with respect to iron. Only a few, rare nucleosynthesis events may have been involved.

Here we determine abundances for Mo, Ru, and other trans-Fe elements for 28 similar stars by matching spectral calculations to well-exposed near-UV Keck HIRES spectra obtained for beryllium abundances. In each of the 26 turnoff stars with Mo or Ru line detections and no evidence for s-process production (therefore old), we find Mo and Ru to be three to six times overabundant. In contrast, the maximum overabundance is reduced to factors of three and two for the neighboring elements zirconium and palladium. Since the overproduction peaks sharply at Mo and Ru, a low-entropy HEW is confirmed as its origin.

The overabundance level of the heavy r-process elements varies significantly, from none to a factor of four, but is uncorrelated with Mo and Ru overabundances. Despite their moderate metallicity, stars in this group trace the products of different nucleosynthetic events: possibly very few events, possibly events whose output depended on environment, metallicity, or time.

1. INTRODUCTION

The heavy-element abundance distributions of metal-poor stars, reviewed by Sneden et al. (2008), can yield critical diagnostics of the objects and environments that formed the material, and its incorporation into Galactic halo and disk stars. For the heaviest elements, these processes are reasonably well understood. In single stars of metallicity below one-thirtieth solar, [Fe/H] < -1.5, elements from barium ($Z = 56$) onward are produced by rapid neutron addition on iron-peak seed nuclei in the r-process. Their elemental abundance ratios are preserved, even though their overall level with respect to iron can be more than an order of magnitude greater or less than the solar level. Only in more metal-rich single stars do elements begin to appear that are created by the s-process (slow neutron capture), in pulsations in intermediate-mass asymptotic giant branch (AGB) stars. The AGB evolutionary time of a few 100 Myr suggests a time delay of this order in the formation of such stars.

In contrast, many processes are invoked for the trans-Fe elements gallium through cadmium ($Z = 31$ to 48). Peterson (2011) provides a summary. Hansen et al. (2012) emphasize that multiple processes are required to explain light trans-Fe abundance ratios, especially at the lowest metallicities. Siqueira Mello et al. (2013) find that electron-capture (O-Ne-Mg) supernovae may contribute the lightest trans-Fe elements, especially if r-process content is extremely low. For molydenum and ruthenium (Mo, Ru; $Z = 42$, 44) in stars with moderate r-process levels, recent work favors the low-entropy domain of a high-entropy wind (HEW) above the neutron star formed in a Type II supernova (e.g. Freiburghaus et al. 1999).

In the solar system, Farouqi et al. (2009) reproduced all seven of the solar isotopes of molybdenum by selecting models from a parameterized grid of HEW calculations. They find it "can co-produce the light p-, s-, and r-process isotopes between Zn ($Z = 30$) and Ru ($Z = 44$) at ... low entropies $S \leq 100$ – 150. Under these conditions, the light trans-Fe elements are produced in a charged-particle (α-) process, including all p-nuclei up to ^{96,98}Ru. ... This nucleosynthesis component is primary."

Support for HEW production in metal-poor stars with low r-process content emerged from observed ratios of the light trans-Fe element yttrium and the heavy r-process element europium (Y, Eu; $Z = 39$, 63). François et al. (2007) noted an anti-correlation between [Y/Eu] and [Eu/Fe], and Roederer et al. (2010) reproduced the [Y/Eu] ratios via HEW models (Farouqi et al. 2010).

Strong confirmation for HEW production in metal-poor stars emerged when Peterson (2011) determined Mo and Ru abundances from Mo II and Ru II lines in ultraviolet spectra of five unevolved stars. Two of these, HD 94028 and HD 160617 with [Fe/H] $= -1.4$ and -1.8, showed [Mo/Fe] $= +1.0$ and $+0.8$, and [Ru/Fe] $= +0.7$ and $+0.6$. Zr ($Z = 40$) was less enhanced, as were the r- and s-process heavy elements Only HEW models have predicted high excesses of the light trans-Fe elements that are confined to this narrow mass range in Z.

Peterson (2011) noted that existing Mo I abundances for >20 field and cluster giants with similarly low heavy r-process content, [Eu/Fe] $< +0.6$, all show [Mo/Fe] $< +0.5$. This rarity of high Mo excesses implied that only

a few distinct nucleosynthesis events produced the light trans-Fe elements in the two extreme turnoff stars.

In this work, we derive abundances for Mo, Ru, and other trans-Fe elements in 28 additional moderately metal-poor turnoff stars. We discuss results for 26 of these, excluding one (HD 106038) that shows mild *s*-process contamination, and one (G 66-30) whose high temperature and broader lines suggest it is a blue straggler. We derive Mo and Ru abundances from the Mo I line at 3864.10Å and the Ru I line at 3498.94Å, lines which were often used in previous analyses of giants. A few stars have only upper limits or marginal detections; for the rest, the two elements exhibit the same excess to ±0.1 dex. In all cases, the mean MoRu abundance is enhanced by a factor of three to six above the solar proportion: $+0.4 \leq$ [MoRu/Fe] $\leq +0.8$.

We also derive and discuss the abundances of the lighter trans-Fe elements strontium, yttrium, and zirconium (Sr, Y, and Zr; Z = 38, 39, 40), plus the heavier element palladium (Pd; Z = 46), the latter analyzed to date in fourteen stars. None of these elements shows enhancements as large as that of Mo and Ru in any star. From this we confirm the low-entropy regime of a HEW as the principal means of production of Mo and Ru in moderately metal-poor turnoff stars.

We measure the overall *r*-process not from europium, but from dysprosium and erbium (Eu, Dy, Er; Z = 63, 66, 68), because the lines of Dy II and Er II are less blended. We find that the *r*-process enhancement varies from none to a factor of four, varying significantly from star to star, implying distinct events.

2. STELLAR SPECTRA

Our data are a subset of the Keck HIRES echelle spectra that Boesgaard et al. (2011, Table 1) obtained to measure beryllium in over a hundred metal-poor stars near the main-sequence turnoff. We selected spectra of stars with metallicities $-2.0 \leq$ [Fe/H] ≤ -1.4 from the 16 runs that followed the Keck CCD upgrade, from September 2004 to July 2010. Currently we have analyzed only the 3440Å – 3950Å portion of the bluest CCD, except for fourteen stars where reductions reached the Pd I line at 3404.579Å.

We reduced all spectra from the raw images in the IRAF[1] environment. We performed bias and dark removal, coadded (with cosmic-ray removal) any multiple spectral images of the same object obtained the same night, extracted orders with removal of sky and local interorder background, corrected the dispersion using concurrent Th-Ar exposures, rectified the continuum with spline fits, and spliced together adjacent orders. The spectra were shifted to zero velocity by cross-correlation against theoretical templates, using the routine *fxcor*.

For the strongest-lined stars, no true continuum could be discerned throughout the blue region. After a preliminary analysis, we re-rectified the continuum by first dividing the extracted echelle spectrum order-by-order by the best-fit theoretical spectrum, itself normalized by dividing by the continuum spectrum included in the calculation (after fitting by hand a pseudocontinuum to the 3860Å – 3900Å Balmer-limit region). We then ran spline fits on the ratio, and divided the extracted echelle orders by the fits. This largely but not entirely removes the continuum suppression due to atomic- and molecular-line blending, provided the the theoretical spectrum is a close match.

[1] IRAF is distributed by the National Optical Astronomy Observatories, which are operated by the Association of Universities for Research in Astronomy, Inc., under cooperative agreement with the National Science Foundation.

3. SYNTHETIC SPECTRAL ANALYSIS

Stellar parameters and abundances were derived by matching each stellar spectral observation to theoretical spectra calculated for each star using an updated version of the Kurucz (1993) SYNTHE program with the stellar models of Castelli & Kurucz (2003). We input a list of molecular and atomic line transitions with wavelengths, energy levels, and gf-values, and a model atmosphere characterized by effective temperature $T_{\rm eff}$, surface gravity log g, microturbulent velocity $V_{\rm t}$, and logarithmic iron-to-hydrogen ratio [Fe/H] with respect to that of the Sun. We calculate the entire spectral region, and compare against each observed spectrum to find the best match. Peterson (2011, Section 4) provides details.

In deriving the stellar parameters, rather than use photometry, we match strengths line-by-line. For this range of line strengths, the 3463.1Å – 3469.2Å region was most useful, with additional Fe II lines and lower-excitation Fe I lines from 3440Å – 3550Å, and the very strong low-excitation Fe I lines at 3820Å – 3830Å. Except for the latter, we used weak lines only.

We started with the Boesgaard et al. (2011, Table 2) values for $T_{\rm eff}$, log g, and [Fe/H]. We checked [Fe/H] from Fe I lines with lower excitation potential $\sim$ 3 eV, then compared Fe I lines of 0.8 – 1.5 eV versus high-excitation Fe I lines to set $T_{\rm eff}$. We then confirmed or altered log g from the match to Fe II lines and the wings of the strong Fe I lines. As these log g indicators always agreed to 0.1 dex and yielded reasonable values, non-LTE effects are evidently small. Peterson et al. (2001) note that this consistency among $T_{\rm eff}$ and log g indicators in metal-poor turnoff stars extends to visible wavelengths and to Balmer lines. It requires the extensive line-list modifications described there, and the use of atmospheric models with no convective overshoot, including our adopted Castelli & Kurucz (2003) models. Where available, the near-UV flux level and slope are matched as well, suggesting the overall temperature scale is reliable.

We simply adopted microturbulent velocities based on stellar parameters, choosing the solar value of 1.0 km/s for main-sequence stars of near-solar $T_{\rm eff}$, 0.9 km/s for cooler main-sequence stars, and 1.1 to 1.2 km/s for progressively hotter and/or lower gravity stars, as suggested from the convection discussion of Castelli et al. (1997).

Table 1 lists the resulting stellar model parameters and abundances. By repeating selected stellar parameter determinations from different starting points, we estimate uncertainties of ±100 K in $T_{\rm eff}$, ±0.2 dex in log g, and ±0.1 dex in [Fe/H]. Due to the low excitation and ionization potentials of the Mo I and Ru I lines, [Mo/Fe] and [Ru/Fe] values rise by ∼0.05 dex for a 100 K rise in $T_{\rm eff}$.

The uncertainty estimates are supported by the agreement of our values with those Boesgaard et al. (2011) found for the same stars. Excluding BD +13 3683, mean differences and 1σ mutual standard deviations of $T_{\rm eff}$,

Table 1
Stellar Parameters and Element Abundances [Element/Fe]

Star	$T_{\rm eff}$	log g	[Fe/H]	$V_{\rm t}$	Mn	Co	Sr	Y	Zr	Mo	Ru	Pd	Nd	Eu
BD -8 4501	6100	4.2	−1.50	1.1	−0.2	0.0	−0.2	0.0	0.3	0.7	0.7	0.2	0.1	0.5
BD -17 484	6300	4.2	−1.50	1.1	−0.2	0.0	−0.1	0.1	0.3	<0.5	0.5		0.0	0.3
BD +4 4551	6000	4.1	−1.30	1.0	−0.3	−0.1	0.0	0.2	0.4	0.6	0.6	0.2	0.0	0.2
BD +7 4841	6000	3.9	−1.50	1.1	−0.3	0.0	0.0	0.1	0.4	0.6	0.6		0.0	0.2
BD +13 3683	6000	4.0	−1.85	1.2	−0.2	0.1	0.0	0.1	0.4	≤0.8	0.8		0.0	0.5
BD +17 4708	6150	3.9	−1.70	1.1	−0.1	0.1	0.0	0.0	0.3	<0.6	≤0.6		0.0	0.4
BD +21 607	6150	4.1	−1.70	1.1	−0.2	0.1	−0.2	0.0	0.2	<0.6	0.6		0.0	0.3
BD +23 3912	5800	3.6	−1.45	1.2	−0.2	0.1	−0.1	0.1	0.3	0.5	0.5	0.2	−0.2	0.1
BD +36 2165	6200	4.1	−1.60	1.1	−0.1	0.0	−0.1	0.0	0.3	<0.5	0.5		0.0	0.4
BD +37 1458	5550	3.6	−1.90	1.2	−0.3	0.0	0.0	0.3	0.5	0.7	0.7		0.1	0.5
BD +42 3607	5900	4.4	−2.10	1.1	−0.3	0.2	0.0	0.0	0.4	<0.6	≤0.6		0.0	0.3
BD +51 1696	5600	4.5	−1.30	1.0	−0.2	0.0	−0.3	−0.1	0.2	0.5	0.5	0.3	0.0	0.5
G 113-9	6200	4.2	−1.60	1.1	−0.4	0.0	0.0	0.2	0.4	0.7	0.7	0.0	0.0	0.0
G 115-49	5900	4.4	−2.10	1.0	−0.2	0.3	−0.3	−0.1	0.3	<0.6	≤0.6		0.0	0.2
G 180-24	6050	4.1	−1.50	1.1	−0.2	0.1	0.0	0.1	0.4	0.6	0.6	0.3	0.0	0.3
G 188-22	6000	4.1	−1.30	1.1	−0.3	−0.1	0.0	0.2	0.4	0.6	0.6		0.0	0.2
G 191-55	6000	4.3	−1.75	1.1	−0.4	0.0	−0.1	0.0	0.3	0.7	0.7	0.3	0.0	0.4
G 192-43	6200	3.9	−1.50	1.2	−0.1	0.0	−0.2	0.1	0.3	0.6	0.6	0.2	−0.1	0.6
G 66-30	6400	4.1	−1.50	1.2	−0.1	0.0	0.0	0.0	0.2	<0.9	<0.9		0.0	0.5
HD 31128	5950	4.2	−1.50	1.0	−0.2	0.0	0.0	0.1	0.3	0.6	0.6		−0.1	0.2
HD 106038	6100	4.2	−1.30	1.1	−0.2	0.1	0.1	0.5	0.6	0.8	0.8		0.3	0.3
HD 108177	6100	4.1	−1.75	1.1	−0.1	0.1	−0.1	0.0	0.3	<0.6	0.6		0.0	0.2
HD 160617	6000	3.8	−1.80	1.2	0.0	0.0	0.0	0.0	0.4	0.8	0.6		0.3	0.4
HD 161770	5650	3.6	−1.60	1.2	−0.3	0.0	−0.1	0.0	0.2	0.5	0.5	0.2	0.0	0.3
HD 188510	5450	4.55	−1.55	0.9	−0.1	0.0	−0.1	−0.1	0.2	0.4	0.4	0.2	0.0	0.3
HD 194598	5900	4.0	−1.20	1.1	−0.1	0.0	−0.3	−0.1	0.2	0.4	0.4	0.1	0.0	0.3
HD 233511	6100	4.3	−1.55	1.1	−0.3	0.1	−0.1	0.1	0.4	0.5	0.5	0.1	0.0	0.0
HD 241253	5750	4.0	−1.30	1.0	−0.1	0.1	0.0	0.1	0.2	0.6	0.6	0.2	0.0	0.3
HD 247168	5700	4.3	−1.60	1.0	−0.2	−0.1	−0.4	−0.2	0.0	0.5	0.5	0.0	0.0	0.3

Note. — Units: $T_{\rm eff}$, K; $V_{\rm t}$, km s^{-1}. Marginal detections and non-detections are indicated by ≤ and < respectively.

log g, and [Fe/H] are 30 K, 0.19 dex, and 0.02 dex, and 154 K, 0.28 dex, and 0.15 dex. However, our temperatures are occasionally >200 K hotter (G 115-49, BD +13 3683, BD +42 3607) or cooler (BD -8 4501, BD +51 1696, HD 241253).

BD +13 3683 is the most deviant star. Our values are higher for $T_{\rm eff}$ by 500 K, for log g by 0.9 dex, and for [Fe/H] by 0.5 dex. The near-UV spectrum of this star is a close match to that of HD 108177, which has the same parameters as those of BD +13 3683 to within the uncertainties. We infer that BD +13 3683 is a binary, a turnoff primary with a cooler companion, and that our reliance on the 3500Å region has led to a higher $T_{\rm eff}$.

4. MOLYBDENUM, RUTHENIUM, AND PALLADIUM ABUNDANCES

For simplicity in the plots below and for better accuracy in the comparison of the Mo and Ru abundances versus those of lighter and heavier elements, we have tabulated the average excess derived from the Mo and Ru lines, instead of individual values for each element. The spectral comparisons presented immediately below indicate that the two lines give abundances that agree to within 0.1 dex whenever both lines are detected.

Figures 1 and 2 compare the calculations based on the parameters in Table 1 to the observations around the Mo I line at 3864.103Å and the Ru I line at 3498.942Å. These regions also show the r-process line of Er II at 3499.103Å, and the s-process lines of Nd II near 3863.4Å.

Figure 1 plots the stronger-lined stars, and Figure 2 shows weaker-lined ones. Figure 2 also includes HD 160617 for reference, comparing a calculation using the updated line list used throughout this work to the UVES pipeline spectrum analyzed by Peterson (2011). For one star in each figure – HD 161770 in Figure 1 and BD -8 4501 in Figure 2 – calculations are also shown in which [Mo/Fe] and [Ru/Fe] values higher and lower by 0.3 dex are adopted. Since the lines are weak and minimally blended, this doubles and halves the line strength.

From this we estimate a measurement uncertainty of ±0.1 dex in all cases where both lines are detected. The uncertainty is ±0.15 dex for four stars where Ru I is detected but Mo I is not: BD −17 484, BD +21 607, BD +36 2165, and HD 108177. It is ±0.2 dex for the three stars where even Ru I is only marginally detected: BD +17 4708, BD +42 3607, and G 115-49. We nonetheless include these stars throughout this discussion.

The mean [MoRu/Fe] value for the 26 stars is 0.58 ± 0.02 dex, an average enhancement of a factor of four above solar. Several stars have enhancements similar to those of the two extreme stars of Peterson (2011), HD 160617 and HD 94028. Consequently, no longer is the incorporation of products from very few nucleosynthesis events necessarily implied for these two stars.

We have not detected an intrinsic spread in the average abundance of Mo and Ru among these 26 stars. The 1σ standard deviation of the individual [MoRu/Fe] values is 0.09 dex, which is attributable to the uncertainties alone. A trend is hinted with metallicity, but it relies heavily on the least certain [MoRu/Fe] values.

In fourteen stars, we also analyzed the Pd I line at 3404.579Å. Fits to that spectral region are shown in Figure 3. Strong-lined stars are in the left panel, and weaker-lined stars in the right. For each star, two abundances for Pd were adopted, [Pd/Fe] = 0.0 and +0.3, a factor-

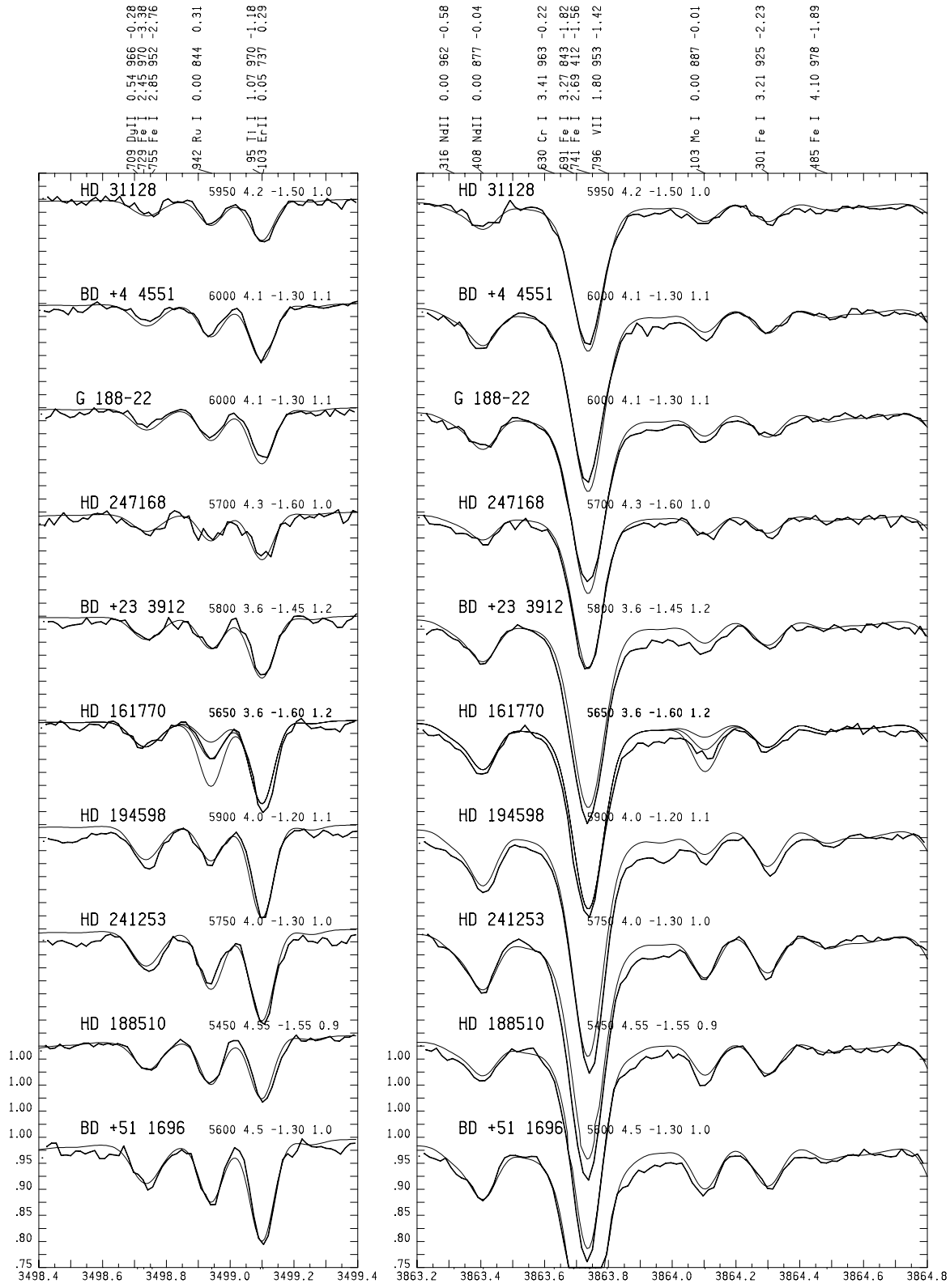

Figure 1. Comparisons are shown between observed and calculated spectra in two spectral regions, with wavelength in Ångstroms given at the bottom. Plots for ten stronger-lined stars are offset vertically by 20% of the normalized continuum; ticks on the y axis indicate 2.5% of this level. The heavy line is the observed spectrum, and the light line the calculated spectrum. Its strongest lines are identified at the top. First are the digits following the decimal place of the line center wavelength, then its species, its lower excitation potential in eV, its strength (stronger lines have lower numbers), and its log gf-value. The star identification from Table 1 is given above each plot. Following it are the stellar parameters adopted for its calculation: $T_{\rm eff}$, log g, [Fe/H], and $V_{\rm t}$. The relative elemental abundances adopted are provided in Table 1. For HD 161770, calculations are also shown with Mo/Ru abundances 0.3 dex higher and lower.

of-two increase. All the observed Pd I lines fall on or within these two values. Consequently, in these stars Pd

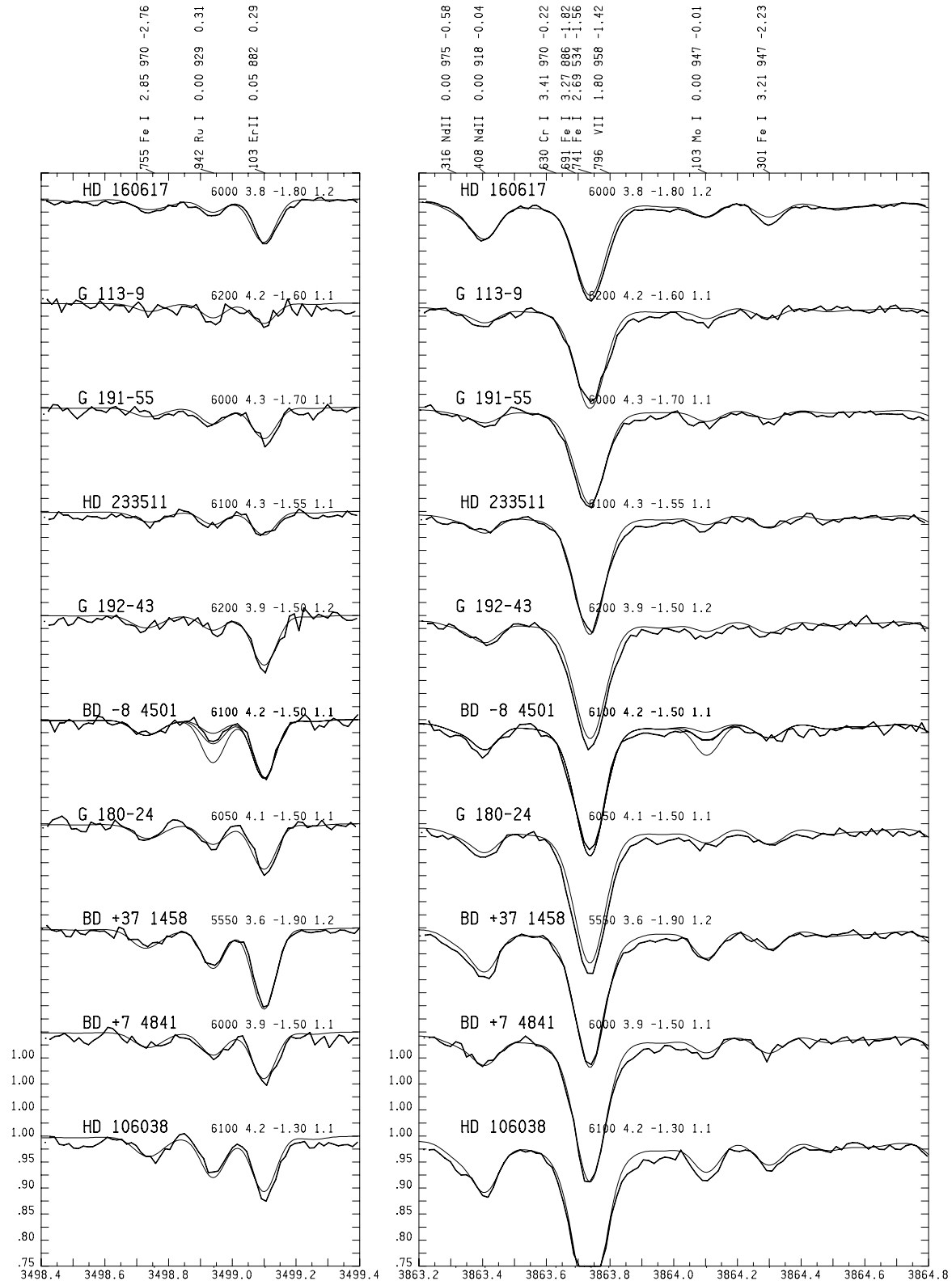

Figure 2. The same comparisons as in Figure 1 are shown for ten weaker-lined stars. Nine are newly analyzed in this work. The top star, HD 160617, analyzed by Peterson (2011), is shown for comparison. As for HD 161770 in Figure 1, calculations adopting Mo/Ru abundances 0.3 dex higher and lower are shown for BD -8 4501.

is always substantially less enhanced than Mo and Ru.

5. HEAVY *S*- AND *R*-PROCESS ABUNDANCES

For the *s*-process indicator we used not lanthanum but neodymium (La, Nd; $Z = 57, 60$), based on the Nd II lines near 3863Å, as the strong La II lines of Peterson (2011) lie redward. We adopted a solar value of log(Nd/(H+He))

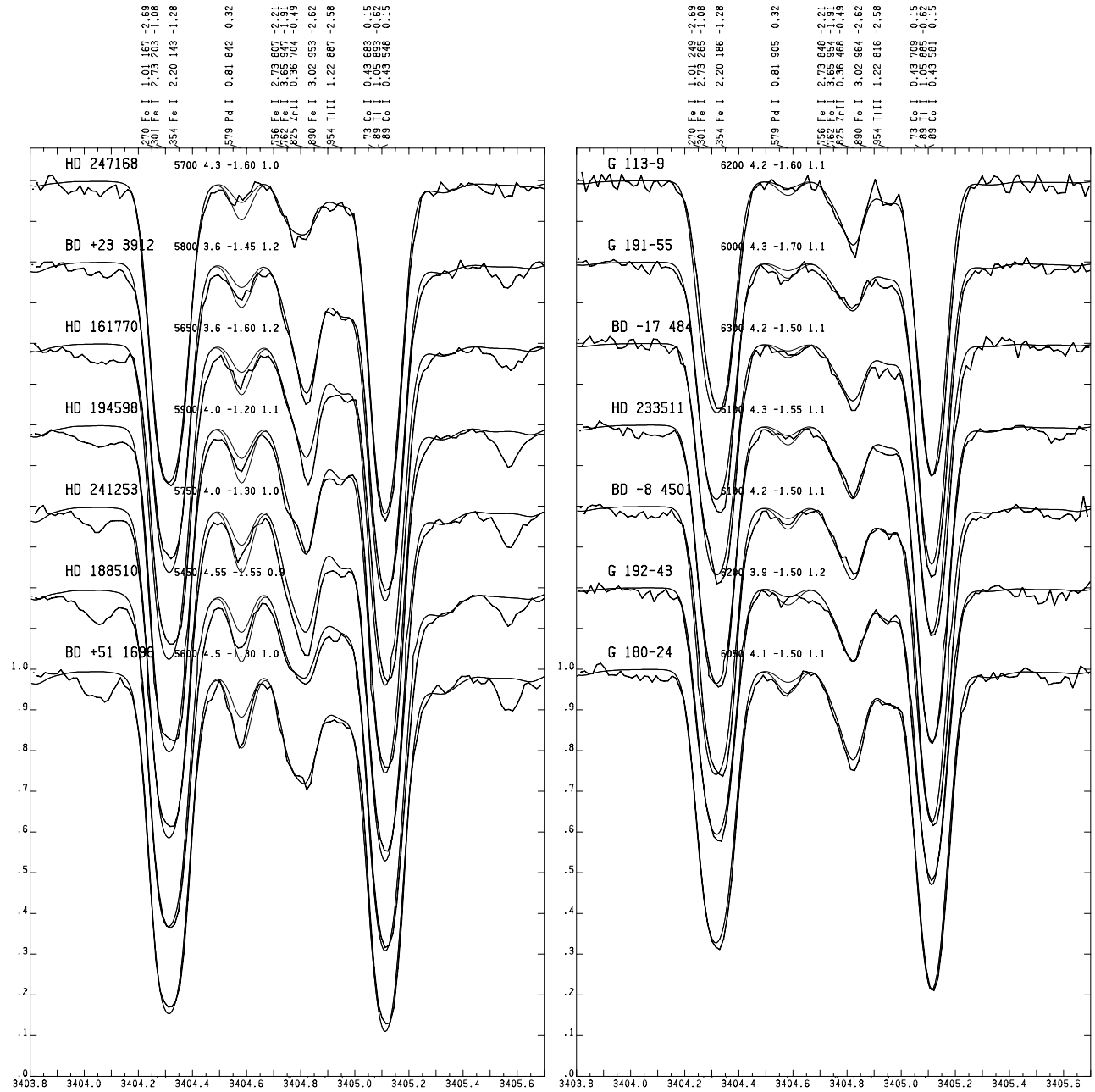

Figure 3. Similar comparisons for seven strong-lined and seven weak-lined stars are shown for the spectral region containing a Pd I line at 3404.579Å. The calculations show two choices for palladium, [Pd/Fe] = +0.0 (solar) and +0.3 (twice solar). The [Pd/Fe] values listed in Table 1 are derived from this plot. They range over $0.0 \leq$ [Pd/Fe] $\leq +0.3$; values as high as those of [Mo/Fe] and [Ru/Fe] are ruled out.

= −10.54.

As seen from Table 1 and directly in Figures 1 and 2, the Nd II lines are detected in all stars. All but three show the solar proportion or higher, [Nd/Fe] ≥ 0.0. Only for [Eu/Fe] $\geq +0.3$ is this expected from an *r*-process contribution alone. For HD 106038, the result [Nd/Fe] = +0.3 is attributed to the *s*-process, because [Eu/Fe] = +0.3 but [Zr/Fe] = +0.6, the highest value of all the 29 turnoff stars. HD 160617, analyzed previously, is the only other star in Table 1 showing [Nd/Fe] > 0.2.

The values of [Sr/Fe], [Y/Fe], and [Zr/Fe] track one another closely. [Sr/Zr] and [Y/Zr] average -0.41 ± 0.02 dex and -0.26 ± 0.01 dex, with 1σ deviations of 0.08 dex and 0.06 dex. Any trend for [Zr/Fe] to follow [MoRu/Fe] is weak. We do see an anti-correlation between [Y/Eu] and [Eu/Fe]: [Y/Eu] = -1.17 × [Eu/Fe] + 0.10, with a scatter of about 0.1 dex about this relationship. For HD 106038, [Y/Eu] is 0.45 dex higher than the trend; we attribute this to its *s*-process enhancement.

For the *r*-process indicator we used the Dy II lines at 3531.707Å and 3536.019Å plus the Er II line at 3499.103Å. We estimate an uncertainty of 0.08 dex in this measurement, based on the comparison of the Dy II and Er II line fits. Figures 1 and 2 confirm that the Er II line is easily detected and extremely well matched.

The Eu II line at 3819.7Å provided a secondary check only, as it is blended by Fe I at 3819.493Å and Cr I at 3819.565Å, and falls on the deep wing of a nearby Balmer line. Our spectral calculations for *r*-process el-

ements are run assuming abundances derived from the Arlandini et al. (1999) r-process fractions. We thus express the Dy/Er r-process abundance excesses in terms of [Eu/Fe], for consistency with other work.

We find a mean [Eu/Fe] = 0.29 ± 0.03 dex. The average r-process enhancement for these 26 stars is then a factor of two higher than solar, and a factor of two lower than the enhancement of Mo and Ru. No correlation is present between the two.

[Eu/Fe] does show a significant intrinsic spread. The observed 1σ spread of 0.14 dex and the 0.08 uncertainty imply an intrinsic dispersion of 0.12 dex. Moreover, in Figure 2, HD 233511 and BD -8 4501 have substantially different Er II line strengths, despite having virtually the same stellar parameters.

6. IMPLICATIONS FOR NUCLEOSYNTHESIS

This work establishes that moderate to high excesses of molybdenum and ruthenium are common among mildly metal-poor stars. Mo and Ru are enhanced similarly, by an average factor of four, but Zr and Pd are always less overabundant. This substantiates HEW as the source in metal-poor stars of the light trans-Fe elements with $Z \sim 44$, as only the low-entropy regime of HEW predicts the sizable overproduction of just these elements.

The lower [Mo/Fe] values previously obtained for giants, using the same Mo I line, remain puzzling. Non-LTE effects or model uncertainties may be worse in giant analysis, as the cooler giant models are more transparent and more susceptible to the effects of convection. Illustrative is the Roederer et al. (2012) analysis of UV and optical spectra of four metal-poor subgiants and giants, yielding $T_{\rm eff}$ values > 200 K cooler than estimates from $V - K$ colors, and Fe I abundances that varied systematically with wavelength by up to 0.3 dex. Our turnoff analyses show no such effects (Sect. 3).

The difference might equally well result from a dependence of low-entropy HEW production on metallicity, since most of the previous analyses are for stars of lower metallicity than these; or on the field halo versus globular-cluster environment, since many previously analyzed giants are members of globular clusters.

Because high molybdenum and ruthenium abundances are typical of moderately metal-poor turnoff stars, exceptionally few nucleosynthesis events are not required for the high values Peterson (2011) found for HD 94028 and HD 160617. However, the group as a whole does show a star-to-star spread in [Eu/Fe]. Either these stars typically did incorporate limited and diverse subsets of the ensemble of nucleosynthetic events, or that ensemble itself depended on local environment, metallicity, or time.

In any case, the oldest halo turnoff stars of roughly one-thirtieth solar metallicity do indeed provide tracers of a range of nucleosynthetic events. The majority of these favored production of Mo and Ru more heavily than did nucleosynthesis at later times. With a larger sample of unevolved stars that span a larger metallicity range, the detailed abundance distributions can be correlated against space motions and metallicities to try to identify the defining characteristics of the progenitor stars, or of the subsequent incorporation of their products, that has led to this nucleosynthetic diversity.

We thank M. Spite and W. Aoki for helpful discussions, and the anonymous referee and a second referee (Chris Sneden) for comments that significantly improved this paper. Critical to this work are observations made with the Keck Observatory HIRES spectrograph, under programs H03aH, H11aH, H30aH, H41aH, H169Hb, H177Hb, and H233Hb (PI A. Boesgaard). We appreciate their expert efforts. The previously-analyzed observation of HD 160617 was made with the ESO Telescope and UVES spectrograph at the Paranal Observatory, under program 065.L-0507(A). This research has made use of the Keck Observatory Archive (KOA), which is operated by the W. M. Keck Observatory and the NASA Exoplanet Science Institute (NExScI), under contract with the National Aeronautics and Space Administration.

REFERENCES

Arlandini, C., Käppeler, F., Wisshak, K., et al. 1999, ApJ, 525, 886, 886
Boesgaard, A. M., Rich, J. A., Levesque, E. M., & Bowler, B. P. 2011, ApJ, 743, 140, 140
Castelli, F., Gratton, R. G., & Kurucz, R. L. 1997, A&A, 318, 841, 841
Castelli, F., & Kurucz, R. L. 2003, in IAU Symposium, Vol. 210, Modelling of Stellar Atmospheres, ed. N. Piskunov, W. W. Weiss, & D. F. Gray, 20P–+
Farouqi, K., Kratz, K., & Pfeiffer, B. 2009, PASA, 26, 194, 194
Farouqi, K., Kratz, K., Pfeiffer, B., et al. 2010, ApJ, 712, 1359, 1359
François, P., Depagne, E., Hill, V., et al. 2007, A&A, 476, 935, 935
Freiburghaus, C., Rembges, J.-F., Rauscher, T., et al. 1999, ApJ, 516, 381, 381
Hansen, C. J., Primas, F., Hartman, H., et al. 2012, A&A, 545, A31, A31
Kurucz, R. 1993, SYNTHE Spectrum Synthesis Programs and Line Data. Kurucz CD-ROM No. 18. Cambridge, Mass.: Smithsonian Astrophysical Observatory, 1993., 18
Peterson, R. C. 2011, ApJ, 742, 21, 21
Peterson, R. C., Dorman, B., & Rood, R. T. 2001, ApJ, 559, 372, 372
Roederer, I. U., Cowan, J. J., Karakas, A. I., et al. 2010, ApJ, 724, 975, 975
Roederer, I. U., Lawler, J. E., Sobeck, J. S., et al. 2012, ApJS, 203, 27, 27
Siqueira Mello, C., Spite, M., Barbuy, B., et al. 2013, A&A, 550, A122, A122
Sneden, C., Cowan, J. J., & Gallino, R. 2008, ARA&A, 46, 241, 241